

## EFFECT OF COMPLEXING AGENTS ON PROPERTIES AND STABILITY OF FeS<sub>2</sub> NANOPARTICLES

F. RETANA, B. KHARISSOV, Y. PEÑA, I. GÓMEZ, T. SERRANO\*  
*Universidad Autónoma de Nuevo León, Facultad de Ciencias Químicas,  
Laboratorio de Materiales I, Av. Pedro de Alba s/n, Ciudad Universitaria,  
C.P. 66455, San Nicolás de los Garza, Nuevo León, México*

FeS<sub>2</sub> nanoparticles were prepared by microwave method using tri-sodium citrate and sodium tartrate as complexing agents to study their effect on the optical properties and stability for 21 days without special storage conditions. FeS<sub>2</sub> nanoparticles showed absorption in the visible range with a single-phase of cubic pyrite and crystallite size around  $17.5 \pm 2.92$  nm. Moreover, nanoparticles showed a low photoluminescence intensity. The FT-IR spectra indicate the presence of chemical bonds around the nanoparticles. FE-SEM images showed spherical shape and size distribution in the range of 15-30 nm depending on the complexing agent. The use of complexing agents modifies the size and shape of FeS<sub>2</sub> nanoparticles influencing the tuning of absorption and emission spectra through a period of time.

(Received January 31, 2020; Accepted July 8, 2020)

*Keywords:* Iron disulfide, Complexing agents, Optical properties, Stability, Microwave synthesis

### 1. Introduction

The use of surface ligands such as complexing agents in the chalcogenides synthesis are useful to modify shape and size for specific applications. Besides, complexing agents may have an effect on agglomeration, degradation and oxidation of chalcogenides [1], which may affect the optical, morphological and electrical properties. Numerous complexing agents have been reported in the synthesis of semiconductors although are being replaced by non-toxic and low-cost complexing agents such as tri-sodium citrate and sodium citrate.

Tri-sodium citrate and sodium tartrate have been extensively used to produce chalcogenide nanoparticles such as CdS [2], PbS [3], CuS [4] and ZnS [5]. Besides, ternary chalcogenides (e.g. AgInS<sub>2</sub> and Zn-Ag-In-S) have been prepared in aqueous medium using complex agents [6]. Tri-sodium citrate and sodium tartrate are complex agents that have pairs of free electrons in the carbonyl group, which stabilizes the semiconductor nanoparticles by electrostatic forces, and also act as a ligand with metallic atoms with free pair of electrons [7-8]. Strong complexing agents play an important role in the synthesis of earth-abundant and stable chalcogenide semiconductors.

FeS<sub>2</sub> has attracted attention as photoactive material due to its abundance, non-toxicity and also, a high annual electricity production potential [9-11]. Moreover, its optical properties such as high absorption coefficient ( $\alpha > 10^5$  cm<sup>-1</sup>), a Shockley-Queisser limit around 31%, , a band gap of 0.95 eV and charge mobility of 360 cm<sup>2</sup> V<sup>-1</sup> s<sup>-1</sup> [12-14] make pyrite a promising candidate for high-efficient and low-cost solar cells that can be expanded in the current market.

Despite the advantages, pyrite has showed some limitations within solar cells since the highest conversion efficiency reported is about 3% [15]. A number of reasons keep pyrite out of high efficiency solar cells from sulfur deficiencies to second phases during the synthesis process such as hexagonal troilite (FeS) and orthorhombic marcasite (FeS<sub>2</sub>) with band gaps of 0.04 eV and 0.34 eV, respectively [16-17], and also the iron oxides formation after synthesis. Iron oxides may affect the optical and electrical properties of FeS<sub>2</sub> causing a low performance efficiency.

---

\* Corresponding author: tserranoq@uanl.edu.mx

In this work, it is investigated the effect of tri-sodium citrate and sodium tartrate on the morphological, optical properties, and influence on the stability of FeS<sub>2</sub> (pyrite) nanoparticles during 21 days. The formation of long-term stable FeS<sub>2</sub> nanoparticles may provide a path in the generation of high efficient, low-cost and stable solar cells based on earth-abundant semiconductors.

## 2. Experimental

### 2.1. Material and reagents

All the chemicals used for the synthesis were analytical grade reagents and used as received. Anhydrous iron (II) chloride (98%) and mercaptopropionic acid (>99 %) were purchased from Sigma Aldrich. Ethylene glycol, acetone (99.7%), ethanol (≥99.8%) and hydrochloric acid (37.4 %) were purchased from DEQ and sodium thiosulfate (99.8%) was obtained from J.T. Baker. Tri-sodium citrate dihydrate (99.3%) and sodium tartrate dihydrate (99.7%) were purchased from Fermont.

### 2.2. Synthesis of pyrite FeS<sub>2</sub> using green stabilizers

The reaction was carried out as follows. In a vessel, 1 mmol of anhydrous iron chloride (II), 4 mmol of complexing agent (tri-sodium citrate or sodium tartrate) and 4.5 mmol of sodium thiosulfate were mixed with 50 mL of ethylene glycol and kept under magnetic stirring for 15 minutes. Then, 4 mmol mercaptopropionic acid (MPA) were added to the solution under continuous stirring. Finally, 7 mL of deionized water was added. Microwave heating was performed on the reaction mixture in cycles of 10 s ON and 30 s OFF at 100% microwave power (1000 W, 2.45 GHz). Solutions reacted with a total heating time of 360 s. Reaction finalized when grayish-black powder appears. The end product was centrifuged and washed several times with deionized water, ethanol and acetone. In order to purify the black powder was washed with hydrochloric acid 2 N. Finally, the product was dried under N<sub>2</sub> flux at room temperature for 15 minutes. Samples were storage for 21 days without special conditions. Samples were kept at room temperature with 8% humidity.

### 2.3. Characterization techniques

Crystalline phase and crystallite size of FeS<sub>2</sub> (pyrite) were recorded by X-ray diffraction (XRD) on a Bruker D2 Phaser with a CuK $\alpha$  radiation ( $K\alpha = 1.54056 \text{ \AA}$ ). Data were collected by scanning from 5° to 90°. Fourier-Transform Infrared (FT-IR) spectra were acquired using a Perkin Elmer Spectrum Two at room temperature in reflectance mode with a resolution of 4 cm<sup>-1</sup>. The absorption spectrum and band gap calculation was characterized by ultraviolet-visible spectrophotometer on a Shimadzu UV-1800. The photoluminescence spectra were collected at room temperature on a Perkin Elmer LS55 with an excitation wavelength of 340 nm. The morphology and distribution size of FeS<sub>2</sub> nanoparticles were given by a field emission scanning electron microscope (FE-SEM), JEOL JSM6701F at an accelerating voltage of 3 kV.

## 3. Results and discussions

### 3.1. Structural properties

X-ray Diffraction revealed the crystal lattice of the dried FeS<sub>2</sub> powders. Figure 1 shows diffraction pattern for the as-prepared FeS<sub>2</sub> for 150 s of total heating and without the presence of complexing agents. Main characteristic reflection peaks of pyrite are observed at 28.5°, 32.9°, 37.1°, 40.8°, 47.3° and 56.3° for (111), (200), (210), (211), (220) and (311) planes, respectively. All the peaks correspond to a pure cubic system of FeS<sub>2</sub> (PDF card 01-071-3840) with a lattice parameter of  $a = 5.416 \text{ \AA}$ . Additional peaks for impurities as FeS (troilite) or FeS<sub>2</sub> (marcasite) were not detected. The average crystallite size was estimated using Debye-Scherrer formula, calculated with the strongest (200) diffraction peak, is  $17.5 \pm 2.92 \text{ nm}$ .

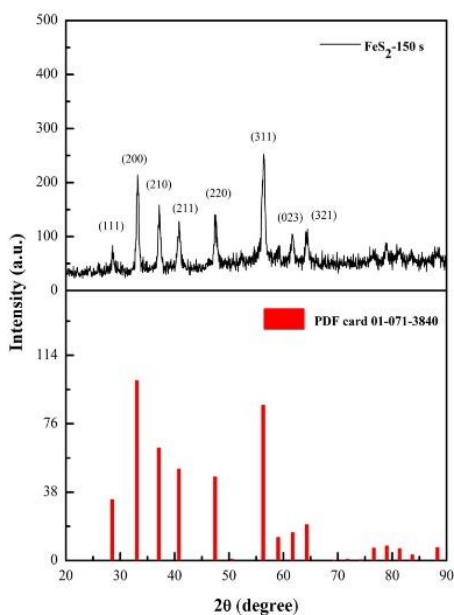


Fig. 1. XRD pattern of FeS<sub>2</sub> nanoparticles.

### 3.2. FT-IR analysis

Fig. 2 shows the FT-IR spectra of FeS<sub>2</sub>, citrate and tartrate capped FeS<sub>2</sub> powders. The broad peak centered around 3495 cm<sup>-1</sup> is attributed to the -OH stretching mode of water. The peaks at around 1650-1700 cm<sup>-1</sup> are assigned to C=O stretching vibrations of the complexing agents. The peaks around 684-700 cm<sup>-1</sup> are related to disulfide bond (S-S) [18-19].

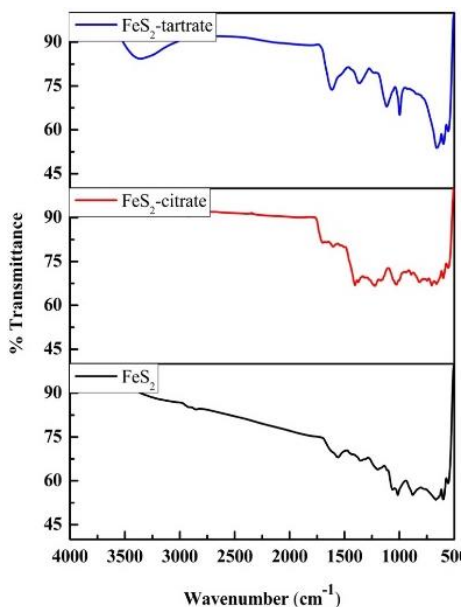


Fig. 2. FT-IR spectra of FeS<sub>2</sub> and citrate and tartrate-capped FeS<sub>2</sub> nanoparticles.

### 3.3. Optical properties

$\text{FeS}_2$  nanoparticles were dispersed in ethanol previous analysis. Fig. 3 displays the room-temperature absorption spectra of  $\text{FeS}_2$  prepared without complexing agents, with tri-sodium citrate, and sodium tartrate. A broad absorbance is observed from 450 to 1100 nm consistent with previous reports in  $\text{FeS}_2$  samples. Samples in presence of complexing agents showed the rise of the absorption band around at 900 nm, which corresponds to the direct bandgap of  $\text{FeS}_2$  [20].  $\text{FeS}_2$  nanoparticles shows a higher absorption, which affects directly the energy band gap of the nanoparticles. Optical band-gap was estimated with Planck's constant and wavelength (900 nm), for all of samples  $E_g$  value is 1.3 eV.

Room temperature photoluminescence of  $\text{FeS}_2$  dispersed in ethanol using a 340 nm excitation in the wavelength from 550 nm to 800 nm is shown in Figure 4. PL spectra illustrated two broad emission peaks at 630 and 720 nm, which are assigned to the excited electron-hole recombination from Fe and S atoms while the second band is relative to S-deficient formation, respectively. The S-deficient can be attributed to  $\text{FeS}_2$  since it is not a perfect stoichiometric compound, where point defects, surface states, and bulk defects are common in the crystal structure, which can induce unusual PL emissions [21]. As a photovoltaic material, it is important to notice that a high PL intensity indicates a higher recombination rate of the electro-hole pairs and short lifetime of the photoluminescence state. Fig. 4 shows the PL spectra collected from the two complexing agents. It is observed a significant change in position and narrowness of the emission bands in PL spectra attributed to the nanostructure sizes are affected by the citrate and tartrate ions. In addition, it is observed that for tartrate samples the emission intensity is lower than citrate samples, which is attributed to the better crystalline quality.

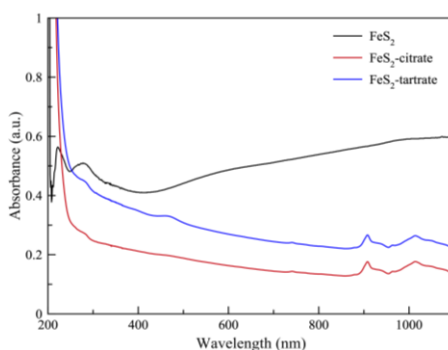


Fig. 3. Optical absorption of  $\text{FeS}_2$  and citrate and tartrate-capped  $\text{FeS}_2$  nanoparticles.

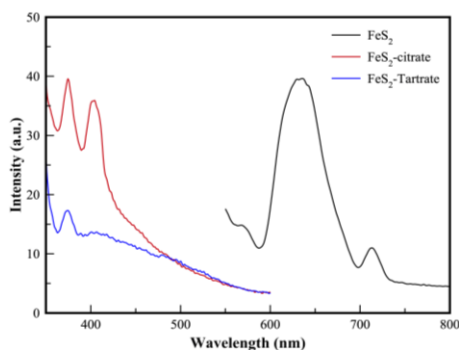


Fig. 4. PL spectra of Optical absorption of  $\text{FeS}_2$  and citrate and tartrate-capped  $\text{FeS}_2$  nanoparticles.

### 3.4. FeS<sub>2</sub> morphology

Fig. 5 (a-c) shows FE-SEM images to reveal morphology and size distribution of FeS<sub>2</sub>. Fig. 5 (a) shows flower sheet-like FeS<sub>2</sub> morphology with a diameter of 35 nm to 65 nm. While in the presence of sodium citrate and tartrate, it is observed the change of morphology from irregular shape into spherical particles. In Fig. 5 (b) particles shows good uniformity with a size distribution of 15 nm to 22 nm. On the other hand, Fig. 5 (c) reveals a size distribution of 25 nm to 30 nm. The different morphology and size between samples can be attributed to the influence of tri-sodium citrate and sodium tartrate on the shape and size of particles [22].

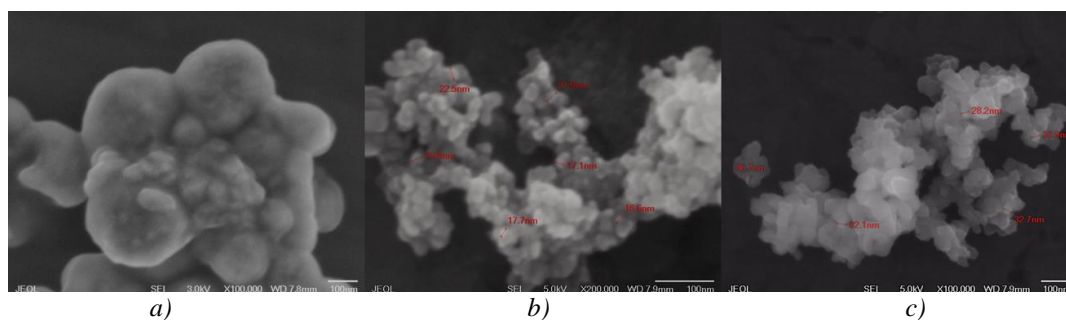


Fig. 5. SEM of (a) FeS<sub>2</sub> nanoparticles and FeS<sub>2</sub> in presence of (b) sodium citrate and (c) sodium tartrate.

### 3.5. FeS<sub>2</sub> stability in presence of citrate and tartrate ions

Additionally, it was studied the influence of citrate and tartrate ions on the optical properties stability against time without special storage conditions. The presence of citrate and tartrate ions in the synthesis of FeS<sub>2</sub> nanostructures required longer reaction time of 300 and 360 s. The samples were kept without a special atmosphere and at room temperature during the 21 days. XRD was used to verify the crystal structure and the presence of iron oxides of the powders through 21 days. Typical XRD patterns of cubic FeS<sub>2</sub> are shown in Fig. 6. In samples with 300 s of total heating is observed the formation of a second phase of Fe<sub>2</sub>O<sub>3</sub>, through the time while samples with 360 s of reaction time did not exhibit impurities during 21 days. Therefore, longer reaction time increases the crystallinity of the samples, which could contribute to better stability on the surface of FeS<sub>2</sub> and to avoid the iron oxides formation.

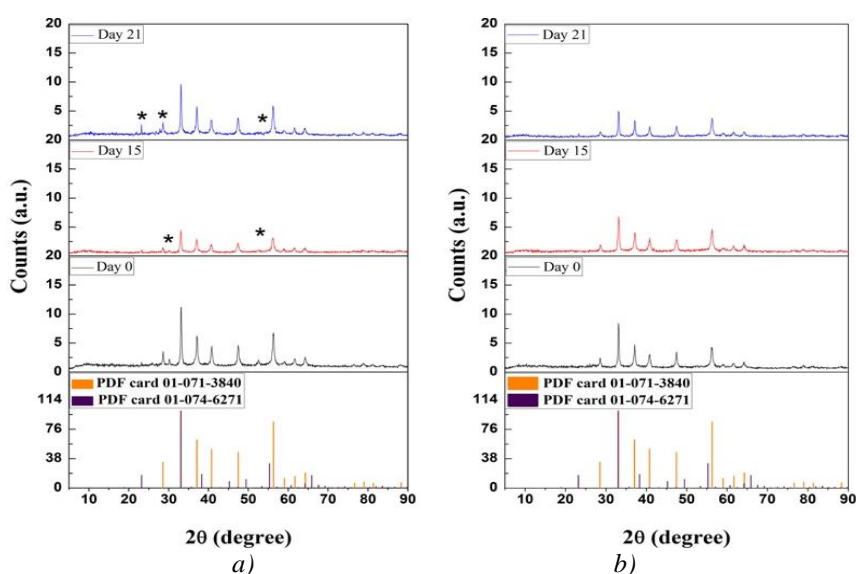


Fig. 6. XRD patterns of FeS<sub>2</sub> at (a) 300 s and (b) 360 s of total heating.

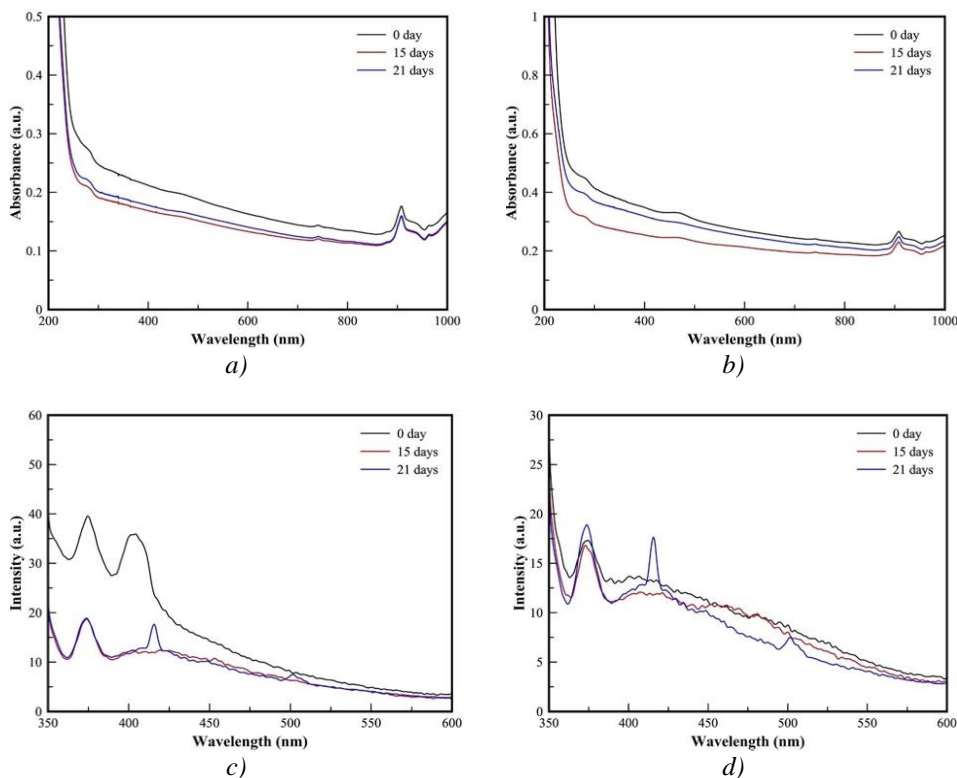


Fig. 7. UV-vis spectra of  $\text{FeS}_2$  in presence of (a) sodium citrate and (b) sodium tartrate for 21 days. PL spectra of  $\text{FeS}_2$  in presence of (c) sodium citrate and (d) sodium tartrate for 21 days.

Fig. 7 (a-d) shows the variation of absorption and emission properties through 21 days. Fig. 7 (a-b) corresponds to the absorption decreased of the samples prepared using green stabilizers. Absorption peak positions are consistent through time without evident change in 21 days for  $\text{FeS}_2$ -citrate samples. In contrast,  $\text{FeS}_2$ -tartrate showed higher intensity but the absorption intensity diminished was more significant through the time, which is attributed to the presence of iron oxides. Fig. 7 (c-d) shows the PL spectra collected from the two different complex agents. 21 days spectra showed evident changes in the intensity, which can be attributed to the presence of iron oxides in the samples. Emission bands at 420 nm and 500 nm corresponds with the typical emission of  $\text{Fe}_2\text{O}_3$  (around 400 nm to 500 nm) [23]. In addition, it is observed that for tartrate samples the emission intensity is lower than citrate samples, which is attributed to the better crystalline quality. Moreover, tartrate samples showed higher stability on the emission intensity.

Different mechanisms in the reaction of pyrite and oxygen have been investigated. Most of the works agree the oxidation on the pyrite surface is due to the incorporation of oxygen on sulfur sites [24], those defects can affect negatively the optoelectronic properties of  $\text{FeS}_2$  devices. Previous studies indicate that citrate and tartrate ions are popular complex agents used in the synthesis of semiconductor nanoparticles due to their low toxicity. It is well known, the free electron pairs in the carbonyl groups of the molecules stabilize the nanoparticles by electrostatic forces.

On the basis of the mentioned results it can be inferred that  $\text{FeS}_2$  nanoparticles are stabilized by MPA between the interaction of thiol groups [25] while citrate or tartrate ions surround the molecules due to the interaction with carboxyl groups. Although during the days the protection of citrate or tartrate ions is lost due to the presence of oxygen in the atmosphere that leads to a strong interaction between Fe-O atoms that produces  $\text{Fe}_2\text{O}_3$  [26].

#### 4. Conclusions

A rapid strategy has been used to obtain cubic FeS<sub>2</sub> (pyrite) using complexing agents through microwave-assisted method. The air-stable FeS<sub>2</sub> nanoparticles exhibited a band gap around 1.3 eV showing a broad absorption peak in visible range. Emission spectra indicate the presence of two broad peaks related to a non-stoichiometric compound.

The stability study suggests the longer reaction time prevents the oxidation through time, while the presence of sodium citrate allows the formation of smaller particles of FeS<sub>2</sub>. Moreover, FeS<sub>2</sub>-tartrate samples exhibit better stability behavior compared with FeS<sub>2</sub>-citrate samples due to the size influencing the absorption and emission properties. This method offers an opportunity to synthesis other air-stable metal chalcogenides of pyrite chemical family without the need of special storage conditions.

#### Acknowledgements

This research (or network) received funding the Mexican Council for Science and Technology (CONACYT) grant PN150 and the PAICYT (UANL) IT1088-19.

#### References

- [1] Y. Zhang, A. Clapp, *Sensors* **11**(12), 11036 (2011).
- [2] C. Selene Coria-Monroy, M. Sotelo-Lerma, C. Martínez-Alonso, P. M. Moreno-Romero, C. A. Rodríguez-Castañeda, I. Corona-Corona, H. Hu, *J. Electron. Mater.* **44**(10), 3302 (2015).
- [3] P. Zhao, J. Wang, G. Chen, Z. Xiao, J. Zhou, D. Chen, K. Huang, *J. Nanosci. Nanotechnol.* **8**(1), 379 (2007).
- [4] X. Chen, J. Yang, T. Wu, L. Li, W. Luo, W. Jiang, L. Wang, *Nanoscale* **10**(32), 15130 (2018).
- [5] A. K. Thottoli, A. K. A. Unni, *J. Nanostructure Chem.* **3**(56), 1 (2013).
- [6] D. S. Mazing, O. A. Korepanov, O. A. Aleksandrova, V. A. Moshnikov, *Opt. Spectrosc.* **125**(11), 773 (2018).
- [7] A. C. S. Samia, J. A. Schlueter, J. S. Jiang, S. D. Bader, C. J. Qin, X. M. Lin, *Chem. Mater.* **18**(22), 5203 (2006).
- [8] L. C. Königsberger, E. Königsberger, P. M. May, G. T. Hefter, *J. Inorg. Biochem.* **78**(3), 175 (2000).
- [9] C. Wadia, A. P. Alivisatos, D. M. Kammen, *Environ. Sci. Technol.* **43**(6), 2072 (2009).
- [10] P. S. Vasekar, T. P. Dhakal, in: A. Morales-Acevedo, "Solar Cells. Research and Application Perspectives", Intech Open, UK, 145 (2013).
- [11] M. Alam Khan, J. C. Sarker, S. Lee, S. C. Mangham, M. O. Manasreh, *Mater. Chem. Phys.* **148**(3), 1022 (2014).
- [12] M. Cabán-Acevedo, M. S. Faber, Y. Tan, R. J. Hamers, S. Jin, *Nano Lett.* **12**(4), 1977 (2012).
- [13] I. N. Yakovkin, N. V. Petrova, *Appl. Surf. Sci.* **377**(1), 184 (2016).
- [14] M. Wang, C. Xing, K. Cao, L. Zhang, J. Liu, L. Meng, *J. Mater. Chem. A.* **2**(25), 9496 (2014)
- [15] L. Luo, W. Luan, B. Yuan, C. Zhang, L. Jin, *Energy Procedia.* **75**, 2181 (2015).
- [16] R. Murphy, D. R. Strongin, *Surf. Sci. Rep.* **64**(1), 1 (2009).
- [17] S. C. Mangham, M. Alam Khan, M. Benamara, M. O. Manasreh, *Mater. Lett.* **97**, 144 (2013).
- [18] A. Dubey, S. K. Singh, B. Tulachan, M. Roy, G. Srivastava, D. Philip, S. Sarkar, M. Das, *RSC Adv.* **6**(20), 16859 (2016).
- [19] M. Khabbaz, M. H. Entezari, *J. Colloid Interface Sci.* **470**, 204 (2016).
- [20] A. Kirkeminda, B.A. Ruzicka, R. Wang, S. Puna, H. Zhao, S. Ren, *ACS Appl. Mater. Interfaces.* **4**(3), 1174 (2012).

- [21] J. Wu, L. Liu, S. Liu, P. Yu, Z. Zheng, M. Shafa, Z. Zhou, H. Li, H. Ji, Z. M. Wang, *Nano Lett.* **14**(10), 6002 (2014).
- [22] S. Middy, A. Layek, A. Dey, P.P. Ray, *J. Mater. Sci. Technol.* **30**(8), 770 (2014).
- [23] M. Lei, R. Zhang, H. J. Yang, Y. G. Wang, *Mater. Lett.* **76**, 87 (2012).
- [24] J. Hu, Y. Zhang, M. Law, R. Wu, *Phys. Rev. B - Condens. Matter Mater. Phys.* **85**(8), 1 (2012).
- [25] H. Zhang, Z. Zhou, B. Yang, M. Gao, *J. Phys. Chem. B.* **107**(1), 8 (2003).
- [26] E. C. Dos Santos, J. C. De Mendonça Silva, H.A. Duarte, *J. Phys. Chem. C.* **120**(5), 2760 (2016).